

Experimental realization of a superfluid stripe phase in a spin-orbit-coupled Bose-Einstein condensate enabled by momentum-space hopping

Thomas M. Bersano,¹ Junpeng Hou,² Sean Mossman,¹ Vandna Gokhroo,¹
Xi-Wang Luo,² Kuei Sun,² Chuanwei Zhang,^{2,*} and Peter Engels^{1,†}

¹*Department of Physics and Astronomy, Washington State University, Pullman, Washington 99164-2814*

²*Department of Physics, The University of Texas at Dallas, Richardson, Texas 75080-3021, USA*

In the past few decades, the search for supersolid-like phases has attracted great attention in condensed matter and ultracold atom communities. Here we experimentally demonstrate a route for realizing a superfluid stripe-phase in a spin-orbit coupled Bose-Einstein condensate by employing a weak optical lattice to induce momentum-space hopping between two spin-orbit band minima. We characterize the striped ground state as a function of lattice coupling strength and spin-orbit detuning and find good agreement with mean-field simulations. We observe coherent Rabi oscillations in momentum space between two band minima and demonstrate a long lifetime of the ground state. Our work offers an exciting new and stable experimental platform for exploring superfluid stripe-phases and their exotic excitations, which may shed light on the properties of supersolid-like states.

Introduction. Supersolids are an exotic phase of matter which simultaneously possess the crystalline properties of a solid and the unique flow properties of a superfluid [1]. Such simultaneous breaking of continuous translational symmetry and U(1) gauge symmetry was first predicted for solid helium [2, 3], but convincing evidence of a supersolid state in this system has remained elusive [4]. In recent years, the experimental realization of spin-orbit coupling (SOC) in ultracold atomic gases [5–17] has opened a new pathway for demonstrating long-sought supersolid-like states [18–30].

The lowest energy band in the SOC dispersion is characterized by two local minima at distinct momenta [5]. For a narrow range of system parameters, mean-field interactions within a Bose-Einstein condensate (BEC) favor a ground state which is composed of a coherent superposition of two plane-wave states at the dispersion minima [22]. This superposition leads to density modulations in real space, or stripes, therefore breaking translational symmetry while maintaining the superfluid phase correlation of a BEC. Such a stripe-phase was initially proposed for SOC BECs where the pseudospins are defined by two atomic hyperfine states [5]. While great experimental progress has been made in exploring the rich physics of such SOC systems, a ground state superfluid stripe-phase has not been observed in this context. The necessary parameter space is prohibitively sensitive to magnetic field fluctuations and the resulting density modulation is weak. However, recent works have attempted to sidestep these difficulties in creative ways, leading to experimental observations of some signatures of superfluid stripe phases in different systems [31–34].

Despite these significant advances, the quest for a robust and long-lived platform for the experimental investigations of stripe-phase properties remains. In this Letter, we show that the superposition of two local band minima to form a supersolid-like ground state can be robustly achieved by means other than atomic interactions.

Specifically, we engineer momentum-space hopping between two local band minima in a SOC BEC driven by a weak optical lattice [35–37]. The coupling between different momenta through static or moving optical lattices has been widely used in ultracold atomic gases for engineering versatile types of physics [38–41], but momentum states involved in such coupling schemes are usually not local band minima and thus have short lifetime. Here such a coupling is applied between two local band minima, hence denoted as hopping, in analogy to the hopping between real-space double wells.

When the decrease of the energy due to momentum-state hopping exceeds the increase of the interaction energy due to density modulation, a stripe-phase is more favorable than a plane-wave state at a single dispersion minimum [42]. In a scheme where SOC is induced by Raman coupling two atomic hyperfine states, this condition can be easily satisfied even for large Raman coupling strengths and detunings, yielding a large parameter region with strong density modulation and spin mixture. While the breaking of continuous translational symmetry is triggered by a weak optical lattice, rather than spontaneously broken, the resulting stripe-phase shares similar physics with an authentic supersolid state [43]. In this sense, the addition of momentum hopping to SOC offers a robustly tunable and long-lived experimental platform for exploring exotic superfluid stripe-phase excitations (e.g. breathing modes, roton excitations and collective dynamics [44]), which may shed light on the properties of supersolid-like states.

In our experiments, we first verify that the spin and momentum composition of our experimentally realized state is consistent with the expected ground state stripe-phase. We then probe the coherent momentum hopping between two SOC dispersion minima by jumping on a weak optical lattice to induce Rabi oscillations. Finally, we investigate the coherence and lifetime of the ground state stripe-phase by quenching the SOC detuning at

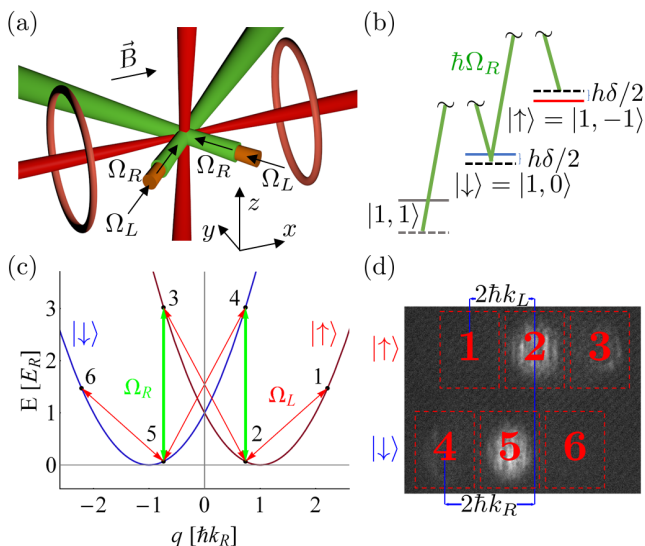


FIG. 1: (a) Schematic of the experimental configuration. A BEC is held in a crossed dipole trap (red) in the presence of a 10 Gauss bias field. Two colinear Raman beams (green) and lattice beams (red) intersect at the BEC position. (b) The Raman coupling scheme. The Raman beams couple the $|1, -1\rangle$ and $|1, 0\rangle$ states of the $F = 1$ manifold with detuning δ . (c) The Raman coupling (green arrows) and the lattice coupling (red arrows) of the relevant momentum states in a rotated spin basis at zero detuning. (d) An example of an experimental measurement using absorption imaging after time-of-flight through a Stern-Gerlach field. The bare states are enumerated to correspond with the marking on the bare-state coupling scheme in (c). Spin-up atoms appear above spin-down atoms due to the Stern-Gerlach field. The occupied momentum states separate horizontally during the time of flight.

different times and observing the population dynamics. These experimental observations of ground states and dynamics are in good agreement with the numerical simulations of the Gross-Pitaevskii equation (GPE), therefore providing significant evidence for the successful production of a stripe-phase ground state.

Spin-orbit coupling with lattice-assisted hopping. We consider the experimental geometry shown in Fig. 1(a). A BEC is prepared in a crossed dipole trap. Two Raman beams are incident on the BEC at 45° angles relative to the x -axis, inducing SOC along the x -direction. These Raman beams couple two atomic spin states $|1, -1\rangle$ and $|1, 0\rangle$ within the $F = 1$ hyperfine manifold, which we will refer to as pseudospin $|\uparrow\rangle$ and $|\downarrow\rangle$ respectively, as shown in Fig. 1(b). This two-photon Raman transition is detuned by δ , while the third spin state ($|1, 1\rangle$) is far off-resonance due to the quadratic Zeeman shift, leaving it effectively decoupled from the other two states.

The coupled spin states are separated in momentum space by $2\hbar k_R$ where the Raman recoil momentum $\hbar k_R$ is the wavevector of the Raman beams projected onto

the x -axis. In a rotated basis, the states are described by a quasi-momentum given by $q = p \pm \hbar k_R$ for the two spin states, where p is the free-particle momentum. The SOC can be visualized as vertical transitions (green) in Fig. 1(c). Diagonalization of the SOC Hamiltonian results in a two-band structure where, for suitable parameters, the lower spin-orbit band features two minima that are located at $q_{\min} = \pm \hbar k_R \sqrt{1 - (\frac{\hbar \Omega_R}{4E_R})^2}$ in single-particle regimes [22]. Here $\hbar \Omega_R$ represents the Raman coupling strength, the recoil energy is $E_R = \hbar^2 k_R^2 / 2m$, and m is the atomic mass of ^{87}Rb .

In addition to the Raman beams, two lattice beams co-propagating with the Raman beams create an optical lattice potential $V_L = 2\hbar \Omega_L \sin^2(k_L x)$ along the x -direction. This static spin-independent lattice can provide a $2\hbar k_L$ momentum-kick while conserving the spin [42]. Such an effect is illustrated by the diagonal couplings (red arrows) marked in Fig. 1(c). The key feature of this configuration is that the wavelength of the lattice beams and the Raman coupling strength are chosen such that the lattice couples the two minima of the lower spin-orbit band, i.e. $\hbar k_L = |q_{\min}|$.

The dynamics of this system can be described by a one-dimensional GPE under the mean-field approximation,

$$i\hbar \frac{\partial}{\partial t} \psi = \left(H_{\text{SOC}} + V_L + \frac{1}{2} m \omega_x^2 x^2 + \frac{g}{2} |\psi|^2 \right) \psi, \quad (1)$$

where ω_x is the trapping frequency along x and $\psi = (\psi_\uparrow, \psi_\downarrow)^T$ is the two-component spinor wavefunction normalized by the average particle number density $n = \int dx \psi^\dagger \psi$. The SOC term is

$$H_{\text{SOC}} = \begin{pmatrix} \frac{1}{2m} (q_x - \hbar k_R)^2 - \frac{\hbar \delta}{2} & \frac{1}{2} \hbar \Omega_R \\ \frac{1}{2} \hbar \Omega_R & \frac{1}{2m} (q_x + \hbar k_R)^2 + \frac{\hbar \delta}{2} \end{pmatrix}. \quad (2)$$

Although it is not obvious in the bare momentum basis, the two spin-orbit band minima are directly coupled in the SOC dressed basis by the weak optical lattice, which we name as “*momentum-space hopping*”.

Ground state phase diagram. The momentum space hopping gives rise to strong density modulations in real-space resulting from a coherent population of both band minima at quasimomenta $\pm \hbar k_L$. A typical ground state profile from GPE simulation is presented in Fig. 2(a). In the absence of SOC, such high density modulation would usually be achieved in deep optical lattices with lattice depths $\hbar \Omega_L \gtrsim 10E_R$, while here $\hbar \Omega_L \approx E_R$ and the strong modulation mainly originates from large Raman coupling [42]. Given the separation of the momentum minima $2q_{\min}$, the real-space distance between the modulation peaks is $\pi/q_{\min} = 0.76 \mu\text{m}$, which is confirmed in the GPE simulations (Fig. 2(a)). Experimentally, we cannot directly observe density modulations at this length scale due to the optical resolution limit of our imaging configuration. Instead, we infer the existence

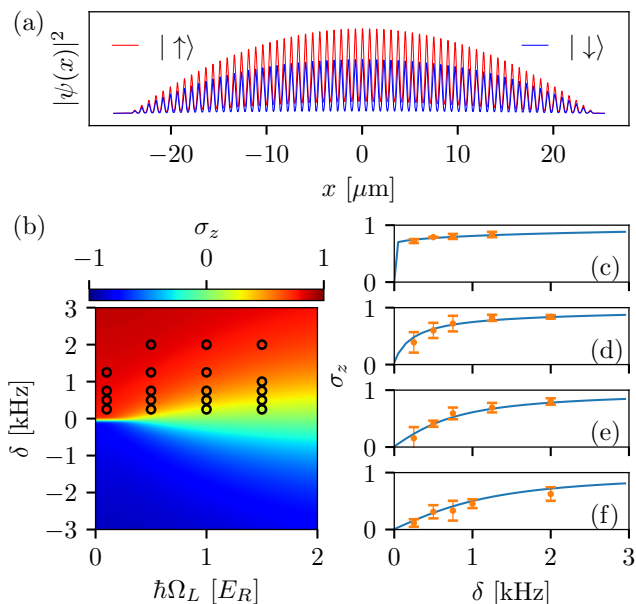


FIG. 2: (a) A numerical example of the stripe ground state density modulations with $|\uparrow\rangle$ shown in red and $|\downarrow\rangle$ shown in blue where $\hbar\Omega_R = 2.7E_R$, $\delta = 250$ Hz, and $\hbar\Omega_L = 1E_R$. (b) Numerical simulation of the ground state spin-polarization phase diagram as a function of SOC detuning δ and lattice coupling strength $\hbar\Omega_L$. The circles indicate the locations experimentally probed in the following subfigures. (c)-(f) Experimental data (dots) and numerical prediction (lines) of spin polarization as a function of Raman detuning for fixed lattice strengths of $\hbar\Omega_L = 0.1$ (c), 0.5 (d), 1.0 (e), and $1.5 E_R$ (f) respectively. All numerics and experiments are done with SOC coupling strength $\hbar\Omega_R = 2.7E_R$. Experimental data points are averages over four measurements with error bars given by statistical error.

of the stripe-phase ground state by verifying other observable parameters, such as the spin polarization of the ground state and the frequency of Rabi oscillations.

We begin by exploring the ground state spin polarization as a function of lattice coupling strength $\hbar\Omega_L$ and SOC detuning δ . After adiabatically dressing the BEC with SOC at a large detuning $\delta = 5$ kHz, the lattice beams are ramped on over 50 ms and then the Raman detuning is adiabatically lowered to a final value. The resulting ground state is imaged and the spin-polarization is measured. The total spin-polarization of the system is given by $\sigma_z = \sum_i s_i N_i / \sum_i |s_i| N_i$, where N_i is the number of atoms in state i with pseudo-spin s_i , which we take to be $1/2$ and $-1/2$ for atoms in hyperfine levels $|1, -1\rangle$ and $|1, 0\rangle$ respectively. These populations N_i are determined through Stern-Gerlach imaging after expansion such that the momentum states separate horizontally, while the spin states separate vertically, as shown in Fig. 1(d).

The experimental data are presented along with the

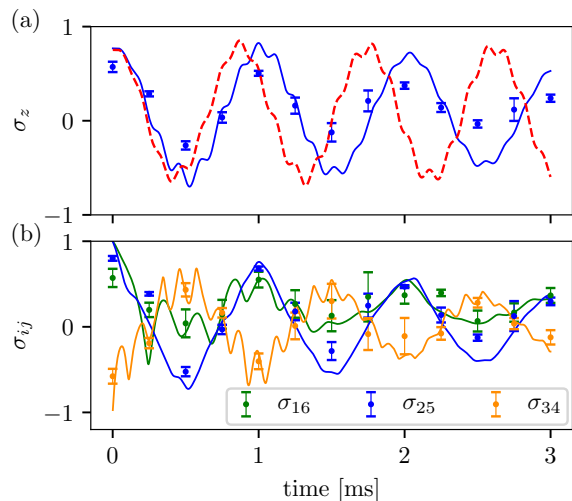


FIG. 3: (a) The Rabi oscillation of the total spin polarization after suddenly jumping on the lattice. Experimental measurements are given by blue points. Blue solid and red dashed lines represent numerical simulations with and without interactions, respectively. (b) The Rabi oscillations between individual spin-momentum channels corresponding to the bare-state basis as marked in Fig. 1(d). The data shown here correspond to SOC strength $\hbar\Omega_R = 2.7E_R$, detuning $\delta = 250$ Hz and lattice strength $\hbar\Omega_L = 1.0E_R$. Experimental data points are averages over four measurements with error bars given by statistical error.

results from numerical simulations in Fig. 2(b-f). The numerically determined ground state phase diagram as a function of SOC detuning and lattice strength, shown in Fig. 2(b), reveals that for small ratios of $|\hbar\Omega_L/\delta|$, nearly all atoms occupy one spin state. As the ratio increases, the two band minima become more evenly populated and the spin-polarization approaches zero. Intuitively, we see a finite SOC detuning energetically favors one spin-state while the lattice coupling mixes the spin-momentum states. A closer observation reveals that the spin polarization changes smoothly (Fig. 2(d-f)) with respect to detuning where the lattice coupling is strong, but shows an abrupt change (Fig. 2(c)) when the coupling is weak. This result is due to the competition between interatomic interaction and lattice coupling [37]. The experimentally determined spin-polarizations are in excellent, quantitative agreement with numerical values (Fig. 2(c-f)), indicating that the physically realized system is consistent with the spin-momentum mixtures which result in the superfluid stripe-phase observed in the numerics.

Coherent Rabi oscillation. The coherent nature of the lattice-induced hopping between two band minima can be experimentally demonstrated by observing Rabi oscillations induced by a sudden quench of system parameters. After adiabatically dressing the BEC with SOC, the lattice beams are jumped on, which initiates an oscillation between the two SOC dispersion minima. After

a certain evolution time, all beams are turned off and the individual spin/momentum states are imaged. The resulting spin polarization oscillates in time as shown in Fig. 3(a). The observed oscillation frequency is in good agreement with the GPE simulation, demonstrating the coherent dynamics of the system. Additionally, Fig. 3(b) shows the same oscillation for particular spin-momentum state pairs as marked in Fig. 1(d), where $\sigma_{ij} = (N_i - N_j)/(N_i + N_j)$. We see good agreement between the experimental values for each of the dominant spin-momentum coupling channels and the corresponding GPE simulation. While the vast majority of the atoms populate the bare states marked 2 and 5, Fig. 3(b) indicates that we are able to observe and resolve the coherent oscillations in the coupled spin-momentum space beyond simple SOC, in agreement with GPE simulation.

To explore the role of particle interactions, Fig. 3(a) shows the results of GPE simulations with and without interactions. A two-level single-particle Rabi oscillation has a frequency given by $\hbar\omega = \sqrt{(\hbar\delta k_L/2k_R)^2 + \tilde{V}^2}$ where $\tilde{V} = \hbar\Omega_L\sqrt{1 - (k_L/k_R)^2}/2$ is the effective coupling strength [42]. With the experimental parameters described in Fig. 3, the single-particle Rabi oscillation period is evaluated to be 0.8 ms, which is consistent with GPE simulation without interaction. The role played by nonlinear effects from interatomic interaction is treated on the mean-field level through a variational method [42]. Intuitively, the density-density interaction, which dominates over spin interaction in ^{87}Rb , costs energy and thus makes it less favorable for the condensate to simultaneously occupy both momentum states. As a result, we expect the interactions reduce the frequency of oscillation and introduce damping effects, which are confirmed by our GPE simulations. We observe strong agreements between numerical simulations with interactions and experimental observations, though the experimental data exhibit stronger damping which is not captured by the mean-field analysis. Some higher frequency, lower amplitude oscillations apparent in both single-particle and interacting cases in Fig. 3 are signatures of the highly detuned couplings within the SOC dressed states. Those high-energy states are coupled with different coupling strengths and are less populated, leading to the small ripples on the overall Rabi oscillation. The Rabi oscillations shown here are driven by a weak lattice which is slightly stronger than the mean field interaction strength. This character may be indicative of the dynamics underlying momentum-space Josephson junctions [37], which is beyond the scope of these experimental observations.

Stripe-phase ground state stability. While previous arguments have indicated that we reliably prepare the appropriate spin-momentum mixtures to achieve a high-contrast stripe-phase, those mixtures must be coherent over a long period of time to produce the expected density modulation for further investigation of dynamical

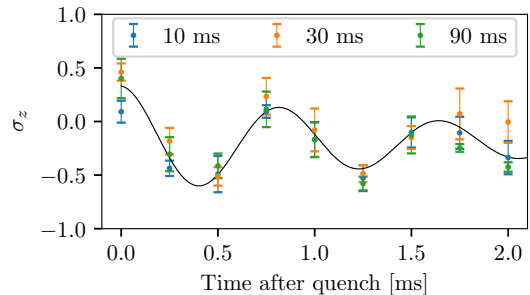


FIG. 4: Detuning quench induced oscillations. A lattice-coupled SOC system is prepared in a ground state where $\hbar\Omega = 2.7E_R$, $\delta = 500$ Hz, and $\Omega_L = 1.0E_R$. The system is held in the ground state for 10 (blue), 30 (orange), or 90 ms (green) before the detuning is quenched from 500 Hz to -500 Hz. Experimental points are averages of four measurements with error bars representing statistical errors and a least-squares fit to a damped harmonic oscillation as a guide to the eye.

properties and excitations of superfluid stripe phases. To study the coherent lifetime of the ground stripe state, we employ quenches of system parameters initiated at various wait times after the preparation of the ground state. The reproducibility of the ground-state quench dynamics provides evidence for the long time phase stability of the spin-momentum mixtures which produces the stripe-phase.

An example of such a quench is a sudden jump of the SOC detuning δ , which induces coherent oscillations of the spin polarization and corresponding momentum states. We begin by preparing the superfluid stripe-phase with $\approx 2 \times 10^5$ atoms and quench δ from 500 Hz to -500 Hz. We perform the quench 10, 30, or 90 ms after the preparation of the ground state and in all cases observe subsequent oscillations of similar amplitude and frequency. Fig. 4 shows the spin-polarization time series after each of the wait times along with a best-fit curve as a guide to the eye. This consistency indicates that the ground state supported by the lattice-coupled SOC is stable in phase and population on the order of at least 100 ms, providing the possibility for investigating long-time dynamics of supersolid-like phases.

Conclusions. In this work, we have demonstrated a robust framework for the production of a high-contrast, long-lived, and tunable ground state stripe-phase in a SOC BEC. By showing quantitative agreement with numerical simulations of the GPE, we have demonstrated that our experimental configuration is able to reliably produce the expected stripe-phase over a broad parameter space. We confirm that the experimental momentum and spin distributions agree with those expected for both the static and dynamic cases and are coherent over long times (~ 100 ms).

The application of optical lattice driven momentum-

space hopping allows for the SOC stripe-phase to exist over a broad parameter space comparing to previous experiments. Therefore, this configuration opens up new possibilities for investigations of excitation dynamics such as roton modes and breathing modes as well as studies of defects or barriers passing through the superfluid stripe-phase. Additionally, we note that such a setup can also be used to realize momentum-space Josephson effects when the lattice coupling strength is weak compared to particle interactions [37].

Acknowledgements. TMB, SM, VG and PE acknowledge funding from the NSF (PHY-1607495). JH, XL, KS, and CZ are thankful for support from NSF (PHY-1505496), AFOSR (FA9550-16-1-0387) and ARO (W911NF-17-1-0128).

* Email address: chuanwei.zhang@utdallas

† Email address: engels@wsu.edu

- [1] M. Boninsegni and N. V. Prokofv, Supersolids: What and where are they? *Rev. Mod. Phys.* **84**, 759 (2012).
- [2] D.J Thouless, The flow of a dense superfluid, *Ann. Phys.* **52**, 403 (1971).
- [3] A. F. Andreev and I. M. Lifshitz, Quantum Theory of Defects in Crystals, *Sov. Phys. JETP* **29**, 1107 (1971).
- [4] Duk Y. Kim and Moses H. W. Chan, Absence of Supersolidity in Solid Helium in Porous Vycor Glass, *Phys. Rev. Lett.* **109**, 109 (2012).
- [5] Y.-J. Lin, K. Jiménez-García, and I. B. Spielman, Spin-orbit-coupled Bose-Einstein condensates, *Nature (London)* **471**, 83 (2011).
- [6] J.-Y. Zhang et al., Collective Dipole Oscillations of a Spin-Orbit Coupled Bose-Einstein Condensate, *Phys. Rev. Lett.* **109**, 115301 (2012).
- [7] C. Qu, C. Hamner, M. Gong, C. Zhang, and P. Engels, Observation of Zitterbewegung in a spin-orbit-coupled Bose-Einstein condensate, *Phys. Rev. A* **88**, 021604(R) (2013).
- [8] A. J. Olson, S.-J. Wang, R. J. Niffenegger, C.-H. Li, C. H. Greene, and Y. P. Chen, Tunable Landau-Zener transitions in a spin-orbit-coupled Bose-Einstein condensate, *Phys. Rev. A* **90**, 013616 (2014).
- [9] C. Hamner, C. Qu, Y. Zhang, J. Chang, M. Gong, C. Zhang, and P. Engels, Dicke-type phase transition in a spin-orbit-coupled Bose-Einstein condensate, *Nat. Commun.* **5**, 4023 (2014).
- [10] P. Wang, Z.-Q. Yu, Z. Fu, J. Miao, L. Huang, S. Chai, H. Zhai, and J. Zhang, Spin-Orbit Coupled Degenerate Fermi Gases, *Phys. Rev. Lett.* **109**, 095301 (2012).
- [11] L. W. Cheuk, A. T. Sommer, Z. Hadzibabic, T. Yefsah, W. S. Bakr, and M. W. Zwierlein, Spin-Injection Spectroscopy of a Spin-Orbit Coupled Fermi Gas, *Phys. Rev. Lett.* **109**, 095302 (2012).
- [12] R. A. Williams, M. C. Beeler, L. J. LeBlanc, K. Jiménez-García, and I. B. Spielman, Raman-Induced Interactions in a Single-Component Fermi Gas Near an s -Wave Feshbach Resonance, *Phys. Rev. Lett.* **111**, 095301 (2013).
- [13] N. Q. Burdick, Y. Tang, and B. L. Lev, Long-Lived Spin-Orbit-Coupled Degenerate Dipolar Fermi Gas, *Phys. Rev. X* **6**, 031022 (2016).
- [14] B. Song, C. He, S. Zhang, E. Hagiyeve, W. Huang, X.-J. Liu, and G.-B. Jo, Spin-orbit-coupled two-electron Fermi gases of ytterbium atoms, *Phys. Rev. A* **94**, 061604(R) (2016).
- [15] L. Huang, Z. Meng, P. Wang, P. Peng, S.-L. Zhang, L. Chen, D. Li, Q. Zhou & J. Zhang, Experimental realization of two-dimensional synthetic spin-orbit coupling in ultracold Fermi gases, *Nat. Phys.* **12**, 540 (2016).
- [16] Z. Meng et al, Experimental Observation of a Topological Band Gap Opening in Ultracold Fermi Gases with Two-Dimensional Spin-Orbit Coupling, *Phys. Rev. Lett.* **117**, 235304 (2016).
- [17] Z. Wu, L. Zhang, W. Sun, X.-T. Xu, B.-Z. Wang, S.-C. Ji, Y. Deng, S. Chen, X.-J. Liu, J.-W. Pan, Realization of two-dimensional spin-orbit coupling for Bose-Einstein condensates, *Science* **354**, 83 (2016).
- [18] T. D. Stanescu, B. Anderson, and V. Galitski, Spin-orbit coupled Bose-Einstein condensates, *Phys. Rev. A* **78**, 023616 (2008).
- [19] C. Wu, I. Mondragon-Shem, and X.-F. Zhou, Unconventional Bose-Einstein Condensations from Spin-Orbit Coupling, *Chin. Phys. Lett.* **28**, 097102 (2011).
- [20] C. Wang, C. Gao, C.-M. Jian, and H. Zhai, Spin-orbit coupled spinor Bose-Einstein condensates, *Phys. Rev. Lett.* **105**, 160403 (2010).
- [21] T.-L. Ho and S. Zhang, Bose-Einstein condensates with spin-orbit interaction, *Phys. Rev. Lett.* **107**, 150403 (2011).
- [22] Y. Li, L. Pitaevskii, and S. Stringari, Quantum tricriticality and phase transitions in spin-orbit coupled Bose-Einstein condensates, *Phys. Rev. Lett.* **108**, 225301 (2012).
- [23] Y. Zhang, L. Mao, and C. Zhang, Mean-field dynamics of spin-orbit coupled Bose-Einstein condensates, *Phys. Rev. Lett.* **108**, 035302 (2012).
- [24] H. Hu, B. Ramachandhran, H. Pu, and X.-J. Liu, Spin-orbit coupled weakly interacting Bose-Einstein condensates in harmonic traps, *Phys. Rev. Lett.* **108**, 010402 (2012).
- [25] T. Ozawa and G. Baym, Stability of ultracold atomic bose condensates with rashba spin-orbit coupling against quantum and thermal fluctuations, *Phys. Rev. Lett.* **109**, 025301 (2012).
- [26] K. Sun, C. Qu, Y. Xu, Y. Zhang, and C. Zhang, Interacting spin-orbit-coupled spin-1 Bose-Einstein condensates, *Phys. Rev. A* **93**, 023615 (2016).
- [27] Z.-Q. Yu, Phase transitions and elementary excitations in spin-1 Bose gases with Raman-induced spin-orbit coupling, *Phys. Rev. A* **93**, 033648 (2016).
- [28] G. Martone, F. Pepe, P. Facchi, S. Pascazio, and S. Stringari, Tricriticalities and quantum phases in spin-orbit-coupled spin-1 bose gases, *Phys. Rev. Lett.* **117**, 125301 (2016).
- [29] X.-W. Luo, K. Sun, C. Zhang, Spin-tensor-momentum-coupled Bose-Einstein condensates, *Phys. Rev. Lett.* **119**, 193001 (2017).
- [30] J. Hou, H. Hu, K. Sun, and C. Zhang, Superfluid-Quasicrystal in a Bose-Einstein Condensate, *Phys. Rev. Lett.* **120**, 060407 (2018).
- [31] J. Li, W. Huang, B. Shteynas, S. Burchesky, F. Top, E. Su, J. Lee, A. O. Jamison, and W. Ketterle, Spin-Orbit Coupling and Spin Textures in Optical Superlattices, *Phys. Rev. Lett.* **117**, 185301 (2016).

- [32] J.-R. Li, J. Lee, W. Huang, S. Burchesky, B. Shteynas, F. Ç. Top, A. O. Jamison, and W. Ketterle, A stripe phase with supersolid properties in spin-orbit-coupled Bose-Einstein condensates, *Nature (London)* **543**, 91 (2017).
- [33] J. Léonard, A. Morales, P. Zupancic, T. Esslinger & T. Donner, Supersolid formation in a quantum gas breaking a continuous translational symmetry, *Nature (London)* **543**, 87 (2017).
- [34] L. Chomaz et al, Observation of roton mode population in a dipolar quantum gas, *Nat. Phys.* **14**, 442 (2018).
- [35] G. I. Martone, T. Ozawa, C. Qu, and S. Stringari, Optical-lattice-assisted magnetic phase transition in a spin-orbit-coupled Bose-Einstein condensate, *Phys. Rev. A* **94**, 043629 (2016).
- [36] T. F. J. Poon and X.-J. Liu, Quantum spin dynamics in a spin-orbit-coupled Bose-Einstein condensate, *Phys. Rev. A* **93**, 063420 (2016).
- [37] J. Hou, X.-W. Luo, K. Sun, T. Bersano, V. Gokhroo, S. Mossman, P. Engels, and C. Zhang, Momentum-Space Josephson Effects, *Phys. Rev. Lett.* **120**, 120401 (2018).
- [38] M. F. Andersen, C. Ryu, Pierre Cladé, Vasant Natarajan, A. Vaziri, K. Helmerson, and W. D. Phillips, Quantized Rotation of Atoms from Photons with Orbital Angular Momentum, *Rev. Lett.* **97**, 170406 (2006).
- [39] M. A. Khamsehchi, C. Qu, M. E. Mossman, C. Zhang, P. Engels, Spin-momentum coupled Bose-Einstein condensates with lattice band pseudospins, *Nat. Commun.* **7**, 10867 (2016).
- [40] E. J. Meier, F. A. An & B. Gadway, Observation of the topological soliton state in the Su-Schrieffer-Heeger model, *Nat. Commun.* **7**, 13986 (2016).
- [41] F. A. An, E. J. Meier, J. Ang'ong'a, and B. Gadway, Correlated Dynamics in a Synthetic Lattice of Momentum States, *Phys. Rev. Lett.* **120**, 040407 (2018).
- [42] See Supplementary Materials for more details.
- [43] G. I. Martone, Quantum Phases and Collective Excitations of a Spin-Orbit-Coupled Bose-Einstein Condensate in a One-Dimensional Optical Lattice, *J. Low Temp. Phys.* **189**, 262 (2017).
- [44] Z. Chen and H. Zhai, Collective-mode dynamics in a spin-orbit-coupled Bose-Einstein condensate, *Phys. Rev. A* **86**, 041604(R) (2012).

Supplementary Materials

Momentum space hopping induced by optical lattices

The analysis starts with a zero-detuned, $\delta = 0$, spin-orbit coupled system with the usual quasimomentum rotation [5] $q = k \pm k_R$. Throughout this Supplementary Material, we use dimensionless units for convenience. We apply a lattice potential,

$$V_{\text{lat}}(x) = 2\Omega_L \sin^2 k_L x = -V(e^{2ik_L x} + e^{-2ik_L x}) + \text{const.}, \quad (3)$$

where $V = \Omega_L/2$. The potential induces the first-order coupling between states with quasimomenta q and $q \pm 2k_L$. The complete 6-level Hamiltonian is given by

$$H = \begin{pmatrix} (q - k_R + 2k_L)^2 & V & 0 & 0 & 0 & 0 \\ V & (q - k_R)^2 & V & \frac{\Omega_R}{2} & 0 & 0 \\ 0 & V & (q - k_R - 2k_L)^2 & 0 & \frac{\Omega_R}{2} & 0 \\ 0 & \frac{\Omega_R}{2} & 0 & (q + k_R)^2 & V & 0 \\ 0 & 0 & \frac{\Omega_R}{2} & V & (q + k_R - 2k_L)^2 & V \\ 0 & 0 & 0 & 0 & V & (q + k_R - 4k_L)^2 \end{pmatrix}, \quad (4)$$

where the first three basis states are spin-up and the latter ones are spin-down, in sequential order. In Fig. 1(c) we label the 6 states of the Hamiltonian basis on the real-spin branches and show couplings between them.

The ground state band of the SOC system possesses two minima at

$$q_{\text{min}} = \pm \sqrt{1 - \left(\frac{\Omega_R}{4}\right)^2}. \quad (5)$$

Consequently, we require $k_L = q_{\text{min}}$ so that the lattice coupling connects the SOC band minima. By using the above relation defining $k_R = 1$ as the unit of momentum, the Hamiltonian becomes

$$H = \begin{pmatrix} (3k_L - 1)^2 & V & 0 & 0 & 0 & 0 \\ V & (k_L - 1)^2 & V & 2\sqrt{1 - k_L^2} & 0 & 0 \\ 0 & V & (k_L + 1)^2 & 0 & 2\sqrt{1 - k_L^2} & 0 \\ 0 & 2\sqrt{1 - k_L^2} & 0 & (k_L + 1)^2 & V & 0 \\ 0 & 0 & 2\sqrt{1 - k_L^2} & V & (k_L - 1)^2 & V \\ 0 & 0 & 0 & 0 & V & (3k_L - 1)^2 \end{pmatrix}. \quad (6)$$

We can rewrite the Hamiltonian in a pseudo-spin basis that diagonalizes the spin-orbit Hamiltonian through a unitary transformation

$$U^\dagger H U = H_d + V H_{nd}, \quad (7)$$

with H_d diagonalized in the transformed basis such that

$$H_d = \text{diag}((3k_L - 1)^2, k_L^2 - 1, k_L^2 + 3, k_L^2 + 3, k_L^2 - 1, (3k_L - 1)^2), \quad (8)$$

and the tunneling terms appear in the off-diagonal part of the Hamiltonian,

$$H_{nd} = \begin{pmatrix} 0 & -\frac{\sqrt{k_L+1}}{\sqrt{2}} & 0 & \frac{\sqrt{1-k_L}}{\sqrt{2}} & 0 & 0 \\ -\frac{\sqrt{k_L+1}}{\sqrt{2}} & 0 & -k_L & 0 & \sqrt{1-k_L^2} & 0 \\ 0 & -k_L & 0 & \sqrt{1-k_L^2} & 0 & \frac{\sqrt{1-k_L}}{\sqrt{2}} \\ \frac{\sqrt{1-k_L}}{\sqrt{2}} & 0 & \sqrt{1-k_L^2} & 0 & k_L & 0 \\ 0 & \sqrt{1-k_L^2} & 0 & k_L & 0 & \frac{\sqrt{1+k_L}}{\sqrt{2}} \\ 0 & 0 & \frac{\sqrt{1-k_L}}{\sqrt{2}} & 0 & \frac{\sqrt{1+k_L}}{\sqrt{2}} & 0 \end{pmatrix}. \quad (9)$$

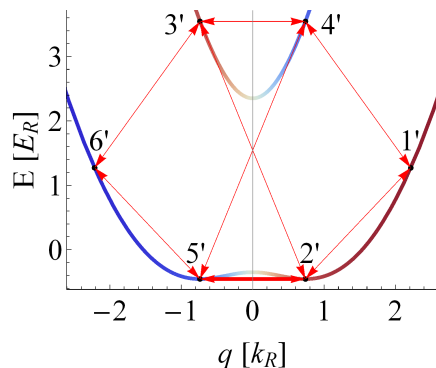


FIG. 5: Dressed lattice coupling diagram. The color coding indicates the relative spin populations where red is predominantly spin-up and blue is strongly spin-down.

The couplings between different states in this pseudo-spin basis are illustrated in Fig. 5. In this basis, $|2'\rangle$ is coupled directly to $|5'\rangle$ with a strength $\sqrt{1 - k_L^2}V$ (the two upper band states, $|3'\rangle$ and $|4'\rangle$, are coupled with the same strength), while $|2'\rangle$ couples to higher excited states with strengths $-\sqrt{\frac{1+k_L}{2}}V$ to $|1'\rangle$ and $-k_L V$ to $|3'\rangle$. Consequently, we expect larger coupling between $|2'\rangle$ and $|5'\rangle$ when k_L is small. If detuning is added into the analysis, we find it scales as $k_L \delta$ in the eigenenergies leads to a coupling of states $|2'\rangle$ to $|4'\rangle$ and $|3'\rangle$ to $|5'\rangle$, i.e., from the lower band to the upper band directly, with a strength $\frac{1}{2}\sqrt{1 - k_L^2}\delta$. This term is dropped since $\delta \ll \Omega_L$ in the dynamics of interest.

Density modulation in ground state

A rough analytic model for the SOC stripe-phase contrast can be derived from [22] where the number density as a function of position is a vertically offset cosine curve with amplitude $n_A = 2\sqrt{n_1 n_2} \Omega_R / (4E_R)$. Then the contrast is defined as $C = 2n_A / (1 + n_A)$, where n_1, n_2 are the fractional density of two momentum states and $n_1 + n_2 = 1$. In Fig. 6(b) we plot the contrast as a function of the Raman detuning for a wide range of n_1/n_2 . At any given Raman coupling, the contrast is maximized when $n_1 = n_2$. At high Raman coupling, a sizable modulation occurs even when the minima are unevenly populated. This is also consistent with our numerical simulations shown in Fig. 6(c), which give the phase diagram of the contrast C .

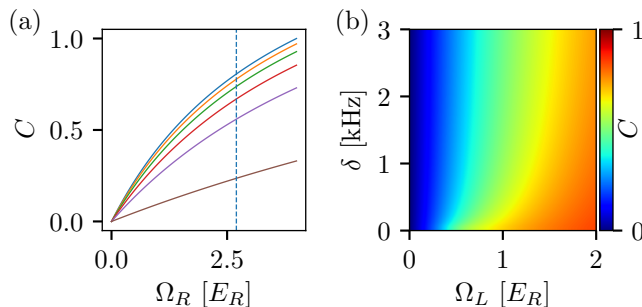


FIG. 6: (a) Fringe contrast for a variety of mixed momentum populations from $n_1/n_2 = \{1, 2, 3, 5, 10, 100\}$, from top to bottom, as a function of SOC strength. A dotted line marks the coupling strength used in this work, $\Omega_R = 2.7E_R$. (b) The fringe contrast as a function of SOC detuning δ and lattice coupling strength Ω_L , where the SOC strength is fixed at $\Omega_R = 2.7E_R$.

Two-state model and quench dynamics

In this section, we study population and phase oscillations between $|2'\rangle$ and $|5'\rangle$ as marked in Fig. 5. For simplicity, we ignore higher-energy states and consider an effective two-level system. To simplify the notation we also drop the

primes in the following discussion. The validity of this 2-level model has been studied thoroughly in previous work [37]. The system dynamics can be approximately described by

$$i\partial_t \begin{pmatrix} C_2 \\ C_5 \end{pmatrix} = (H_0^{\text{eff}} + H_I^{\text{eff}}) \begin{pmatrix} C_2 \\ C_5 \end{pmatrix}, \quad (10)$$

where the effective single particle Hamiltonian H_0^{eff} is given by

$$H_0^{\text{eff}} = -\tilde{\delta}\tau_z + \tilde{V}\tau_x = \omega(-\cos\alpha\tau_z + \sin\alpha\tau_x) \quad (11)$$

with $\tilde{\delta} = \delta k_L/2$, $\tilde{V} = V\sqrt{1 - k_L^2}$, $\tan\alpha = \tilde{V}/\tilde{\delta}$ and $\{\tau\}$ are Pauli matrices. The interaction part is

$$H_I^{\text{eff}} = 2g_G \begin{pmatrix} |C_5|^2 & 0 \\ 0 & |C_2|^2 \end{pmatrix}, \quad (12)$$

where $g_G = ng(1 - k_L^2)$. Rewriting $C_j = N_j e^{i\theta_j}$, $j = 2, 5$, we can recast the 2-level model into two classical equations of motion

$$\partial_t z = -\sqrt{1 - z^2} \sin\phi, \quad (13)$$

$$\partial_t \phi = \frac{g_G}{\tilde{V}} z + \frac{z}{\sqrt{1 - z^2}} \cos\phi + \frac{1}{2} \frac{k_L \delta}{\tilde{V}}, \quad (14)$$

where $z = (N_2 - N_5)/(N_2 + N_5)$, $\phi = \theta_2 - \theta_5$ and time has been rescaled according to $t \rightarrow 2\tilde{V}t$. To observe interaction effects like self-trapping, we typically require $\tilde{\delta}/\tilde{V} \ll 1$ and $g_G/\tilde{V} \gg 1$, which are outside the parameter space we consider in the experiments. When $g_G/\tilde{V} \ll 1$, we simply have a coherent Rabi oscillation with frequency $\omega = \sqrt{\tilde{\delta}^2 + \tilde{V}^2}$. In the experiment, we study the dynamics mainly in the intermediate region (i.e., $\Omega_L \gtrsim 1$ and consequently $g_G/\tilde{V} \lesssim 0.5$). Although strong interaction effects cannot be observed, changes in the periodicity still reveal the important role played by interaction in the dynamics.